Research Article

Journal of Physical Organic Chemistry

Received: 23 January 2008, Revised: 14 April 2008, Accepted: 25 May 2008, Published online in Wiley InterScience: 21 July 2008

(www.interscience.wiley.com) DOI 10.1002/poc.1409

DFT studies on the mechanism of Pd(II)-catalyzed intermolecular 1,2-diamination of conjugated dienes

Youqing Yu[a], Wei Shen[a], Jinsheng Zhang[a], Rongxing He[a] and Ming Li[a]*

The reaction mechanism of the palladium(II)-catalyzed addition of urea to dienes to form 1,2-diamine was studied using the B3LYP density functional theory (DFT) method. The results indicate that the first C—N σ-bond formation is the rate-determining step, and that the covalent bonds are formed favorably by the terminal carbon atoms of dienes and nitrogen atom. The Pd(NCMe)-catalyst may significantly lower the energy barrier of the rate-determining step from the nonligand Pd(II)-catalyst counterpart. The results are in strong support of a recent experiment.

Supporting information may be found in the online version of this article.

Keywords: Pd(II)-catalyzed; DFT; diamination reaction; reaction mechanism

INTRODUCTION

Vicinal diamines are very important functional moieties which are present in various biologically active compounds and have also been widely used as chiral control elements in asymmetric synthesis.[1–3] Diamination of olefins presents an attractive strategy for the synthesis of vicinal diamines. On the other hand, several catalytic routes have also been investigated. Various metal-free[4,5] or metal-mediated[6,7] processes have been developed and metal-catalyzed diaminations have also been reported.[8] Moreover, although transition metal-catalyzed hydroamination[9,10] and oxidative dehydroamination[11,12] have been extensively developed in recent years, transition metal-catalyzed alkene 1,2-diamination is still a challenge.[13] Recently, Booker-Milburn and his co-workers reported intermolecular diamination of dienes catalyzed by palladium(II) complexes (Scheme 1).[14]

Beginning with the reaction of isoprene with urea under appropriate conditions, the reaction can generate regioisomeric diene-urea products **1a** and **1b**. The reactions are interesting because Pd(II)-catalyzed intermolecular 1,2-diamination can produce the major products **1a** (**1a/1b** up to 96%).

There are several mechanisms proposed to account for the amination reaction catalyzed by Pd such as the Pd(0)-catalyzed diamination reaction mechanism by Yian Shi and his co-workers,[15] Pd(II)-catalyzed intramolecular diamination reaction mechanism by Streuff and his co-workers,[16] and Pd-catalyzed oxidation amination of conjugated olefins by Ji Min Lee.[17] Nevertheless, the mechanism of Pd(II)-catalyzed diamination reaction remains unclear and is the subject of this paper.

In view of the interesting catalytic process, it is necessary to theoretically study in more detail about the reaction mechanism. In this paper, we investigated the mechanism of the intermolecular 1,2-diamination reaction by density functional theory (DFT) methods. Based on the mechanism proposed by other researchers in Pd(II)-catalyzed amination reaction and Wacker-type process, we presented a mechanism to account for the intermolecular 1,2-diamination reaction, which is shown in Scheme 2.

Many interesting questions arise when we compare the reaction mechanism of Scheme 2. Among dienes, which of them have two double C=C bonds? If the C—N σ-bond in the main product comes from the Pd(0)-catalyzed diamination reaction between the substituted C=C double bond and N, as reported by Yian Shi, why does the unsubstituted C=C double bond also react with N to form the C—N bond in its main product in the diamination reaction reported by Booker-Milburn? If ligand dissociation of $Pd(NCMe)_2$ can occur, which intermediate of Pd complexes is favorable as an active catalyst? The objectives of this work are to address these important questions with the DFT at the B3LYP level by examining the structural and energetic aspects of various possible reaction pathways. We hope that the findings presented in this paper would help scientists in designing new catalysts for this reaction.

Computational details

Geometry optimizations have been performed via DFT[18,19] of the B3LYP method. Frequency calculations at the same level of theory have also been performed to confirm the characteristics of all the optimized structures as minima or transition states.

* *Correspondence to: M. Li, Department of Chemistry, Southwest University, Chongqing 400715, P.R. China.*
E-mail: liming@swu.edu.cn

a *Y. Yu, W. Shen, J. Zhang, R. He, M. Li*
Department of Chemistry, Southwest University, Chongqing 400715, P.R. China

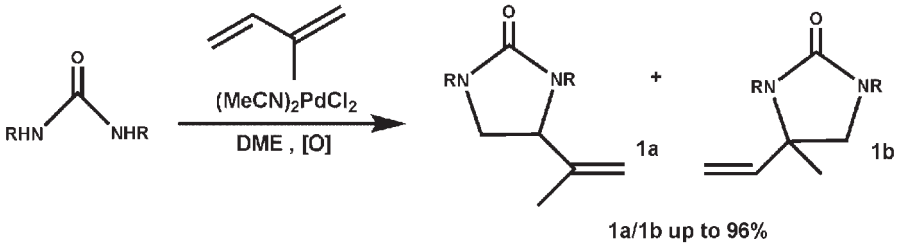

Scheme 1.

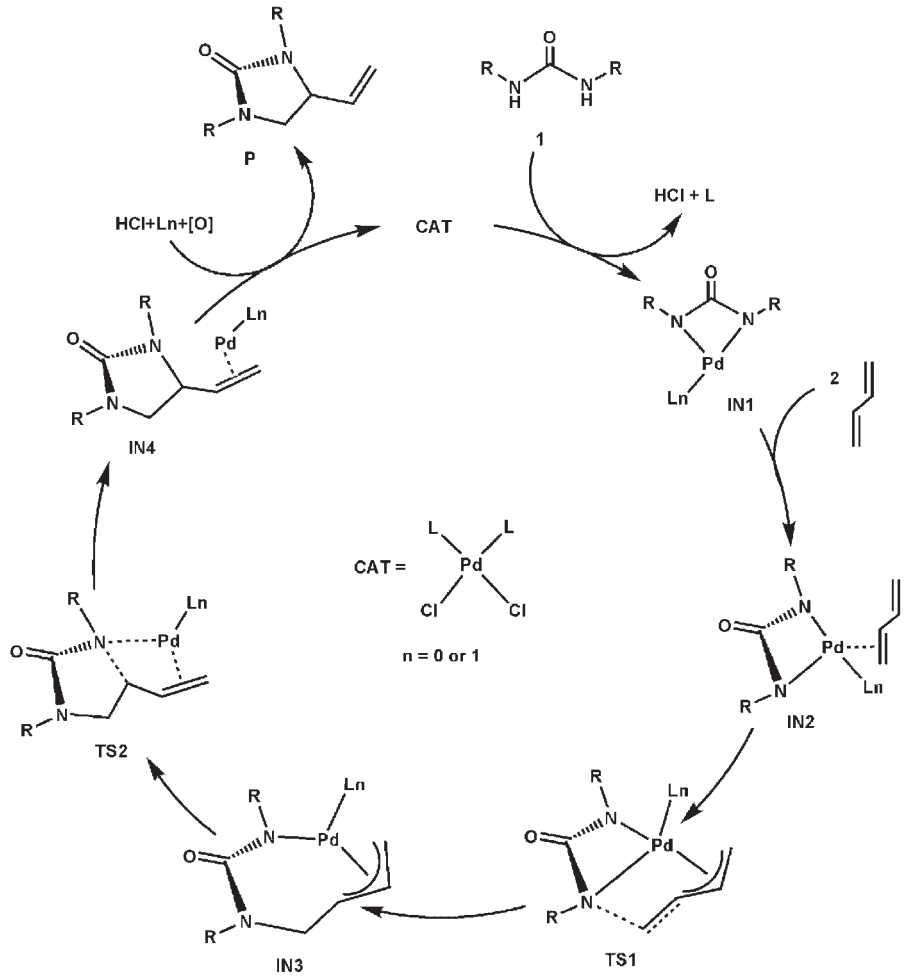

Scheme 2. Proposed mechanism for the intermolecular 1,2-diamination reaction

Calculations of intrinsic reaction coordinates (IRC)[20] were also performed on transition states to confirm that such structures are indeed connecting two minima. The effective core potentials (ECPs) of Hay and Wadt with a double-ζ valence basis set (Lanl2DZ)[21–23] were used to describe Pd atom, while the standard 6–31+g*[24] basis set was used for C, H, O, and N atoms. All calculations were performed with the Gaussian 03 software package.[25] The vibrational analysis and the natural bond orbital (NBO) analysis[26–34] were performed at the same computational level. In addition, the electron densities at the bond critical points (BCP) and the ring critical points (RCP) for the selected bond of some species were calculated by employing the AIM2000 program package.[35] The completely topological analyses are performed for all the compounds to obtain detailed bonding character. The BCPs denoted as (3, −1), which represent saddle points in the electron densities between two atoms are examined for all the bonds.

Molecular orbital (MO) compositions and the overlap populations were calculated using the AOMix program.[36,37] The analysis of the MO compositions in terms of occupied and unoccupied fragment molecular orbitals (OFOs and UFOs, respectively) and the analysis of the construction of orbital interaction diagrams were performed using AOMix-CDA.[38]

RESULTS AND DISCUSSION

As shown in Scheme 2, the Pd(II)-catalyst (**CAT**) coordinates with urea (**R1**) and undergoes ligand dissociation to form **IN1**, HCl, and ligand. From **IN1**, the diene (**R2**) coordinates with Pd, followed by a C—N bond formation to generate **IN3**. Another C—N bond formation then occurs to give birth to **IN4**. To complete the catalytic cycle, **IN4** reacts with HCl, oxidant, and ligand to regenerate **CAT** and produce products. In the first step of the catalytic cycle, the number of the eliminated ligand might be **1** or **2**. Therefore, the catalytic process has two distinctive manifolds: Pd-ligand and Pd as an active catalyst. We also proposed a catalytic cycle catalyzed by Pd-L_2, but the stabilized intermediate and transition cannot be located in this pathway. In our DFT study, we used 1,3-diethylurea as a model for **R1** and isoprene for **R2**. In this paper, '**C1**' denotes the pathways catalyzed by Pd, and '**C2**' by Pd-L.

Mechanism of Pd-catalyzed reactions

The intermolecular 1,2-diamination reaction is a process in which the Pd–urea complex, **C1-IN1**, through transition states (**C1-TS1** and **C1-TS2**), offers a Pd product-complex (**C1-IN4**). There are four structures of intermediate **C1-IN2**, which depends on the relative orientation of C═C double bond of **R2**, and the followed intramolecular C—N σ-bond formation can occur through eight channels. In this paper, two favorable channels, **C1-1-1** and **C1-3-2**, are involved, which lead to the major and the minor products, respectively. The NBO charges and Wiberg bond orders of intermediate and transition states are shown in Table 1. The structures of other channels can be found in Figs S1–S6 and their relative energies in Table 1.

In **C1-IN1** (Fig. 1), the Pd—N1—C1—N2 moiety is on a plane. The optimized Pd—N1 bond is 2.031 Å and the C1—N1 bond is 1.397 Å. The η^2 and η^4 type geometries of **C1-IN2** were considered when **R2** coordinates with **C1-IN1**. Due to the σ-bond bend, the η^4 type geometries are much larger than η^2 type in energies when Z-isoprene coordinates with **C1-IN1**. Furthermore, the transition states of C—N bond formation followed by Z-isoprene η^4 type geometries cannot be located. Although E-isoprene coordinates with **C1-IN1** to form η^4 type complexes which are more stable than η^2 type complexes (about 8 kJ/mol lower), the barriers of the rate-determining step are higher (about 6 kJ/mol higher). Therefore, we just discuss the channels that only one C═C π-bond coordinates with **C1-IN1**.

In **C1-IN2-1**, there is an obvious interaction between Pd and C4═C5 (the Pd—C4 and Pd—C5 bond distances are 2.267 and

Table 1. The NBO charges δ, Wiberg bond orders P_{ij}, and electron density $\rho(r)$ at the BCPs for species in the **C1-1-1** and **C1-3-2**

Species	Atom	δ	Bonds	P_{ij}	Species	Atom	δ	Bonds	P_{ij}
C1-IN2-1	Pd	0.65	Pd–N1	0.50	**C1-IN2-3**	Pd	0.65	Pd–N1	0.52
	C4	−0.53	Pd–N2	0.60		C6	−0.11	Pd–N2	0.59
	C5	−0.30	Pd–C4	0.25		C7	−0.53	Pd–C6	0.19
	N1	−0.61	Pd–C5	0.21		N1	−0.59	Pd–C7	0.24
	N2	−0.51	C4–C5	1.63		N2	−0.52	C6–C7	1.59
C1-TS1-1-1	Pd	0.67	Pd–N1	0.33	**C1-TS1-3-2**	Pd	0.65	Pd–N1	0.26
	C4	−0.26	Pd–N2	0.49		C6	−0.74	Pd–N2	0.63
	C5	−0.45	Pd–C5	0.27		C7	0.15	Pd–C7	0.04
	N1	−0.70	C4–C5	1.34		N1	−0.72	C6–N2	0.42
	N2	−0.55	C4–N2	0.47		N2	−0.48	C6–C7	1.23
C1-IN3-1-1	Pd	0.61	Pd–N1	0.33	**C1-IN3-3-2**	Pd	0.53	Pd–N1	0.54
	C4	−0.28	Pd–C5	0.58		C4	−0.43	Pd–C4	0.00
	C5	−0.23	Pd–C6	0.18		C5	−0.23	Pd–C5	0.01
	C6	−0.06	Pd–C7	0.33		C6	0.05	Pd–C7	0.74
	C7	−0.545	C4–C5	1.03		C7	−0.51	C4–C5	1.98
	N1	−0.56	C4–N2	0.97		N1	−0.62	C6–N2	0.94
	N2	−0.77	C6–C7	1.53		N2	−0.54	C6–C7	1.00
C1-TS2-1-1	Pd	0.39	Pd–N1	0.18	**C1-TS2-3-2**	Pd	0.46	Pd–N1	0.28
	C4	−0.27	Pd–C5	0.23		C4	−0.61	Pd–C4	0.26
	C5	−0.12	Pd–C6	0.25		C5	−0.28	Pd–C5	0.02
	C6	−0.14	Pd–C7	0.36		C6	0.06	Pd–C7	0.38
	C7	−0.54	C4–C5	1.03		C7	−0.37	C4–C5	1.68
	N1	−0.53	C5–N1	0.51		N1	−0.65	C6–N2	0.94
	N2	−0.64	C6–C7	1.55		N2	−0.54	C7–N1	0.52
C1-IN4-1-1	Pd	0.16	Pd–N1	0.00	**C1-IN4-3-2**	Pd	0.20	Pd–N1	0.01
	C4	−0.28	Pd–C5	0.01		C4	−0.57	Pd–C4	0.42
	C5	−0.08	Pd–C6	0.36		C5	−0.38	Pd–C5	0.41
	C6	−0.10	Pd–C7	0.39		C6	0.09	Pd–C7	0.00
	C7	−0.55	C4–C5	0.98		C7	−0.23	C4–C5	1.59
	N1	−0.53	C4–N2	0.96		N1	−0.58	C6–N2	0.94
	N2	−0.58	C6–C7	1.57		N2	−0.58	C7–N1	0.96

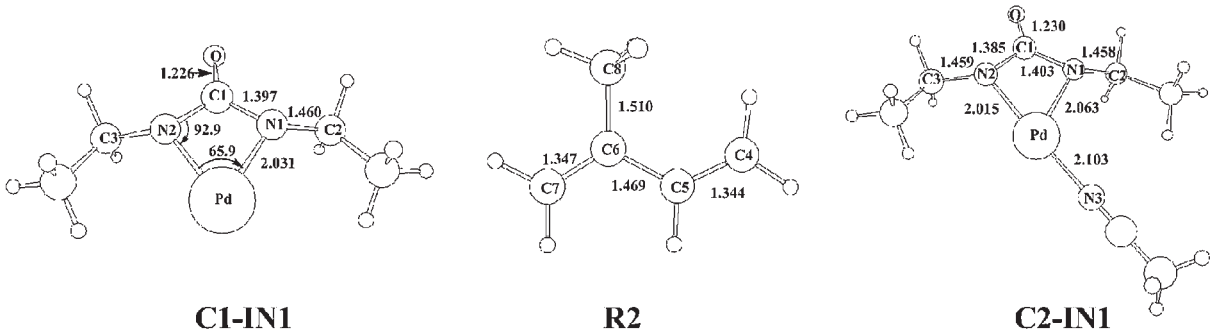

Figure 1. B3lyp/6–31+g* calculated structure of **C1-IN1**, **R2**, and **C2-IN1**

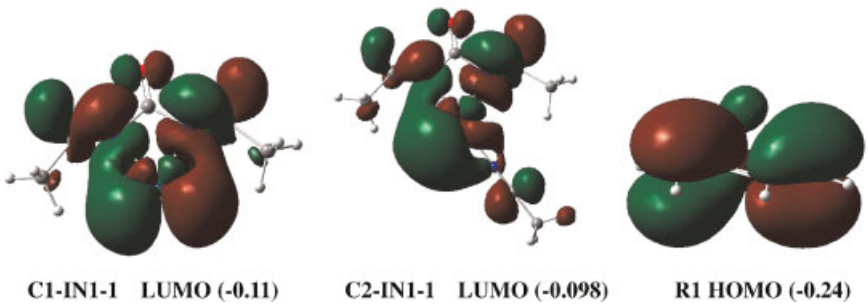

Figure 2. B3lyp/6–31+g* calculated LUMO of **C1-IN2-1** and **C2-IN2-1**, HOMO of **R1**. The energies of orbitals are given in eV

2.309 Å, respectively). The LUMO (π^*) energy of **C2-IN1-1** is −0.11 eV and the HOMO (π) energy of **R2** is −0.24 eV (Fig. 2). The lower energy gap between the two molecular orbitals make them easier to coordinate with. Due to the crowded configuration of **C1-IN2-3**, the difference in bond length between Pd—C6 and Pd—C7 in **C1-IN2-3** (0.083 Å) is larger than that between Pd—C5 and Pd—C6 in **C1-IN2-1** (0.042 Å), and the NBO charge difference between C6 and C7 in **C1-IN2-3** (0.42) is larger than that between C4 and C5 in **C1-IN2-1** (0.23).

The structures of the transition states for the first σ_{C-N} bond formation **C1-TS1** are shown in Figs 3 and 4. In **C1-TS1-1-1**, C4—C5—Pd—N2 forms a four-membered ring and the electron density of RCP is 0.042. The bond distance between C4 and N2 is 2.036 Å, which indicates the tendency to form σ-bond. It can be testified by the Wiberg bond index $P_{ij(N2—C4)}$ (0.47) and the electric density of BCP (0.074) (Fig. 5). The bond distances of Pd—C6 and Pd—C7 are 2.314 and 2.615 Å, respectively, while those of P_{ij} are 0.17 and 0.11. It suggests that the interaction

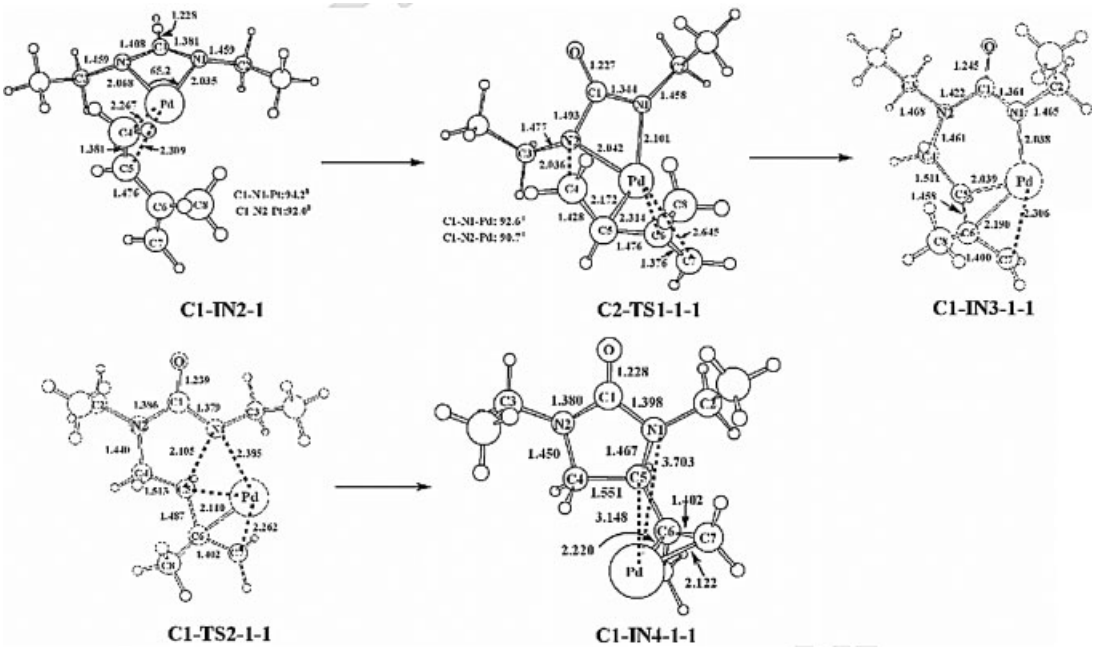

Figure 3. B3lyp/6–31+g* calculated structures of **C1-1-1**

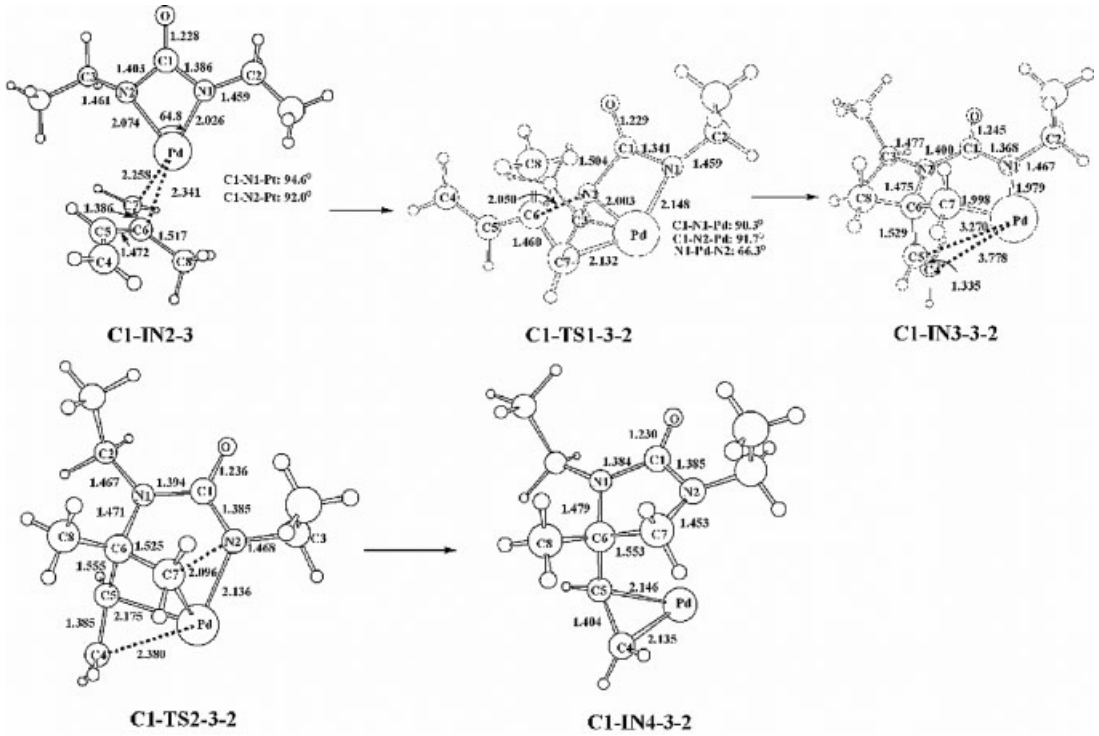

Figure 4. B3lyp/6–31+g* calculated structures of **C1-3-2**

between Pd and C6═C7 is weakened. In the next step they can form π_3^4 bond easily, which agrees with the supposition of experiment. The π_3^4 bond configuration prevents the occurrence of 1,4-addition reaction. The bond distances of Pd—N1 and Pd—N2 are 2.101 and 2.042 Å, respectively, which are slightly longer than those in **C1-IN1-1-1**.

Based on NBO analysis, second-order perturbation of donor–acceptor interactions is used to estimate the strengths of the donor–acceptor interactions of the NBOs. The larger stabilization energy implies stronger interaction between donor and acceptor. In **C1-TS1-3-2**, C6—C7—N2—Pd also forms a four-membered ring, and the configuration is very similar to the four-membered ring in **C1-TS1-1-1**. The NBO analysis of **C1-TS1-1-1** shows that C5 coordinates with Pd by the lone pair of electrons to form π-back-donation bond and the stabilization energy of $LP_{C5} \rightarrow$ N2—C4 is quite large (88.78 kcal/mol). However, in **C1-TS1-3-2**, the Pd *d*-orbital interacts with the C7 *p*-orbital to form σ-bond, and the largest stabilization energy of the bond N2—C4 comes from the π-bond C4═C5 (17.85 kcal/mol). Moreover, there is obvious steric interaction between the substituted groups of N2 and C4═C5. All of these indicate that the formation of C4—N2 σ-bond is easier in **C1-TS1-1-1** than in **C1-TS1-3-2**. The computed energy barriers of **C1-TS1-1-1** and **C1-TS1-3-2** are 144.40 and 160.24 kJ/mol, respectively.

The geometries of **C1-TS1** are similar to **C1-IN2**, which indicate that they are early transition states. The relative higher energy barrier shows that the C—N σ-bond formation step is the rate-determining step for this reaction channel.

In **C1-IN3-1-1**, Pd—N1—C1—N2—C4—C5 form a six-membered ring, the bond distance of N2—C4 is 1.461 Å and P_{ij} is 0.97, which indicates N2—C4 is σ-bond. It can be seen from Fig. 3 that the interaction between Pd and C6═C7 in **C1-IN3-1-1** is stronger than in **C1-TS1-1-1**. The bond distances of Pd—C5, Pd—C6, and Pd—C7 are 2.038, 2.190, and 2.306 Å, respectively. The bond lengths of C5—C6 and C6—C7 are 1.468 and 1.400 Å, respectively. These results suggest that Pd is coordinate with the π_3^4 bond of C5, C6, and C7, whereas, in **C1-IN3-3-2**, the bond distances of Pd—C4 and Pd—C5 are 3.270 and 3.778 Å, respectively, and the long distance indicates that Pd only coordinates with C6 instead of π_3^4 bond. From Fig. 6, we can

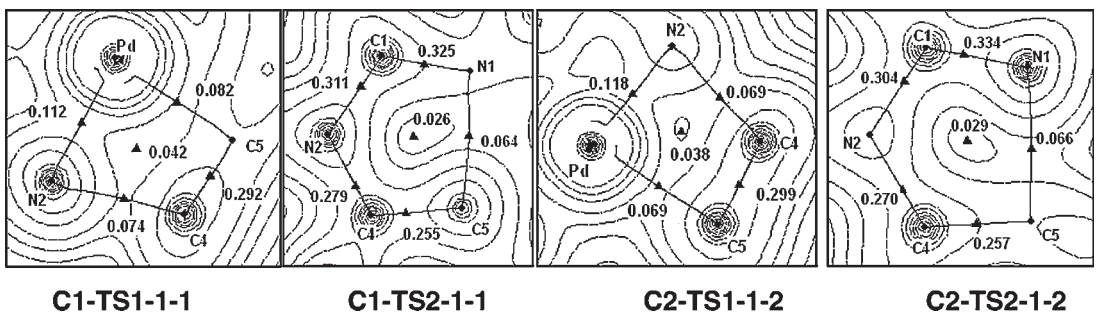

Figure 5. Two-dimensional electron density contours for all the transition states of pathway **C1-1-1** and **C2-1-2** (including electron densities of some selected BCPs and RCPs)

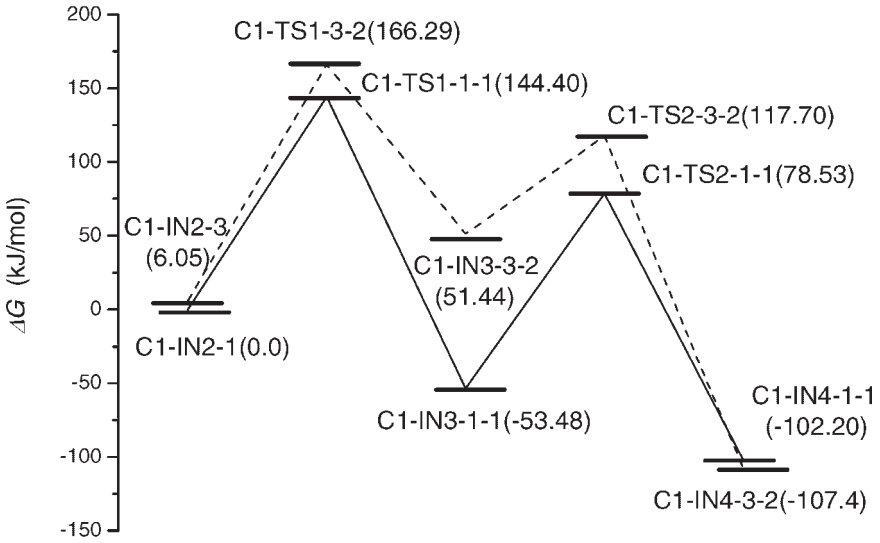

Figure 6. B3lyp/6–31+g* calculated relative free energies for **C1-1-1** and **C1-3-2**. The energies are given in kJ/mol

see that **C1-IN3-1-1** is more stable than **C1-IN3-3-2** (relative energies are −53.48 and 51.44 kJ/mol, respectively), and **C1-IN2-3-2** (relative energy is 6.05 kJ/mol) is more stable than **C1-IN3-3-2**. Therefore, the pathway from **C1-IN2-3-2** to **C1-IN3-3-2** is difficult to occur, which agrees with the experimental result.

C1-IN3, through another intramolecular C—N σ-bond formation, produces the product-catalyst complex **C1-IN4**. In **C1-TS2-1-1**, the transition state involves a N1—C1—N2—C4—C5 five-membered ring and the electron density of RCP is 0.038. The C5···N1 bond distance is 2.106 Å; P_{ij} is 0.51; the electron density of BCP is 0.064. With these results, it demonstrates that N1 and C5 have the tendency to form σ-bond. The bond distances of Pd···N1 and Pd···C5 are 2.381 and 2.385 Å, respectively, and their P_{ij} are 0.23 and 0.18, respectively. It indicates that the interaction between them is very weak. In the product-catalyst complexes **C1-IN4**, Pd coordinates with C═C and it can regenerate the catalyst by releasing product.

An overview of the channels catalyzed by Pd suggests that the favorable pathways are those in which the terminal C atom of isoprene reacts with the N atom to form C—N σ-bond and the first σ_{C-N}-bond formation is the rate-determining step. However, from the energy viewpoint, the high barriers of those rate-determining steps indicate that the channels catalyzed by Pd are difficult to occur.

Mechanism of Pd(NCMe)-catalyzed reactions

The catalytic cycle catalyzed by Pd(NCMe) is similar to that catalyzed by Pd, which involves 16 pathways depending on the relative C═C orientation coordinated with Pd. As mentioned

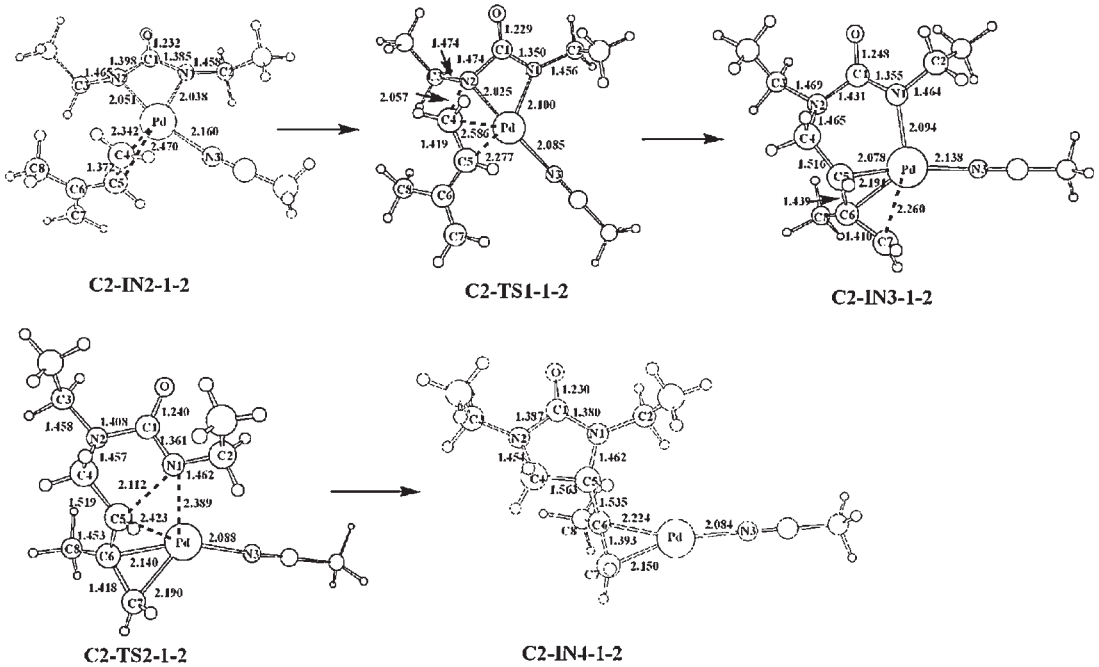

Figure 7. B3lyp/6–31+g* calculated structures of **C2-1-2**

Journal of Physical Organic Chemistry

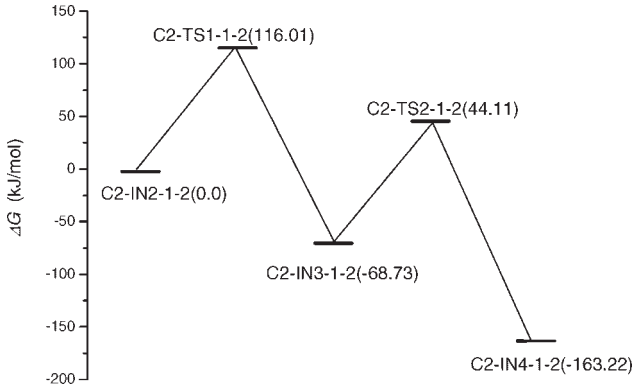

Figure 8. B3lyp/6–31+g* calculated relative free energies (in kJ/mol) for **C2-1-2**

above, the pathways of the terminal C atom, which react with N atom to form C—N σ-bond are favorable. Hence, those pathways of β-C, which react with the N atom are not involved in the reaction cycle. Furthermore, only the favorable channel **C2-1-2** is discussed. The structures of the intermediate and transition states of other channels are illustrated in Figs S7–S13.

The structures of the intermediate and transition states in **C2-1-2** are shown in Fig. 7. In **C2-IN2-1-2**, Pd coordinates with C4═C5. The bond lengths of Pd—C4 and Pd—C5 are 2.342 and 2.470 Å, respectively, and their P_{ij} are 0.20 and 0.16, respectively. The structure of the transition state **C2-TS1-1-2** is similar to that of **C1-TS1-1-1**. The main difference between them is in the bond distances of Pd—C5, Pd—C6, and Pd—C7 (2.172, 2.314, and 2.615 Å in **C1-TS1-1-1**, 2.277, 3.210, and 4.042 Å in **C2-TS1-1-2**, respectively). These results show that the interaction between Pd and C6═C7 is very weak in **C2-TS1-1-2**.

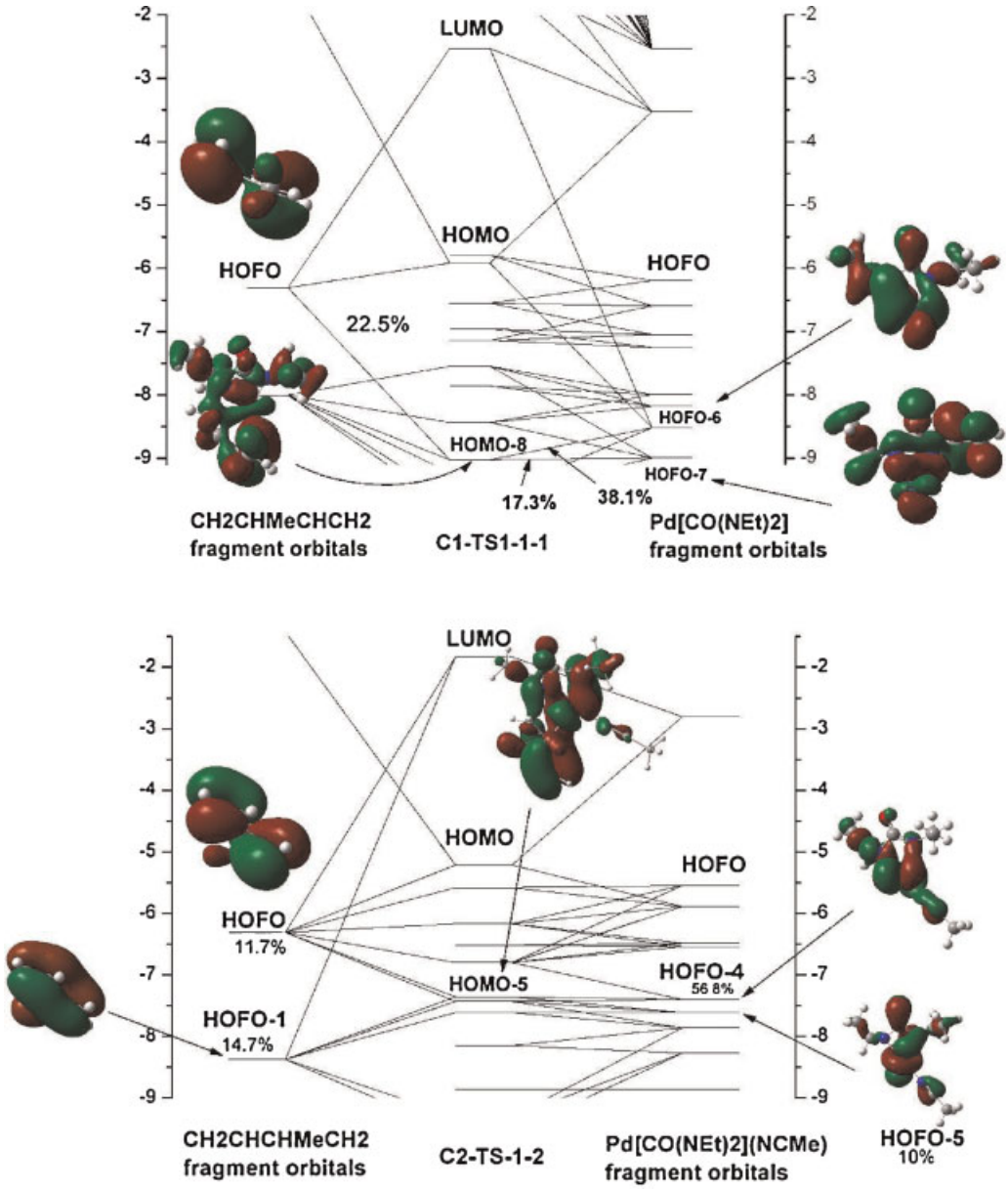

Figure 9. The orbital interaction diagram in **C1-TS1-1-1** and **C2-TS1-1-2** (the AOMix-CDA calculation, based on B3LYP/6–31+g* results). The corresponding FO contributions greater than 5% are illustrated

It can be seen from the energy profile (Fig. 8) that **C2-TS1-1-2** is the rate-determining step of this channel. Compared with **C1-TS1-1-1** (144.40 kJ/mol), the energy barrier of **C2-TS1-1-2** (116.01 kJ/mol) is lower.

In order to understand the details of the C—N bond formation, *AOMix* program was performed to analyze transition states **C1-TS1-1-1** and **C2-TS1-1-2** (see Fig. 9). In AOMix analysis, the structure of **C1-TS1-1-1** is separated into isoprene (fragment 1) and Pd[CO(NEt)2] (fragment 2), and **C2-TS1-1-2** is separated into isoprene (fragment 1) and Pd[CO(NEt)2](NCMe) (fragment 2), respectively. In **C1-TS1-1-1**, the orbital which has the tendency to form C4—N2 σ-bond is HOMO-8, composed of 22.5% $HOFO_{isoprene}$, 38.1% HOFO-$6_{Pd[CO(NEt)2]}$, and 17.4% HOFO-$7_{Pd[CO(NEt)2]}$. The energy difference between $HOFO_{isoprene}$ and HOFO-$6_{Pd[CO(NEt)2]}$ is 2.22 eV/mol while the energy difference between $HOFO_{isoprene}$ and HOFO-$7_{Pd[CO(NEt)2]}$ is 2.68 eV/mol. In **C2-TS1-1-2**, the orbital which has the tendency to form C4—N2 σ-bond is HOMO-5, which mainly comes from 11.7% $HOFO_{isoprene}$, 14.7% HOFO-$1_{isoprene}$, 56.8% HOFO-$4_{Pd[CO(NEt)2](NCMe)}$, and 10.0% HOFO-$5_{Pd[CO(NEt)2](NCMe)}$. The highest energy difference among them is only 0.78 eV/mol. The low orbital energy difference of fragments indicates that the orbital between fragments is easy to overlap, and easy to form C4—N2 σ-bond. Comparing **C2-TS1-2** with **C1-TS1-1-1**, we can see that C4—N2 in **C2-TS1-2** is easier to form σ-bond. Inspecting Figs 5 and 7, the lower energy barrier (116.01 kJ/mol) in **C2-TS1-2** leads to this step which is easier to occur.

The structures of **C2-IN3-1-2**, **C2-TS2-1-2**, and **C2-IN4-1-2** are all similar to channel **C1-1-1**. The energy barrier of the second C—N bond formation is also obviously decreased (112.84 kJ/mol for **C2-TS2-1-2**), and the released energy (163.22 kJ/mol) is much higher than that of **C1-TS1-1-1** (102.20 kJ/mol). Obviously, the reaction catalyzed by Pd(NCMe) is more favorable.

CONCLUSION

In summary, the intermolecular diamination reactions of ureas and dienes catalyzed by Pd(II) complexes discovered by Booker-Milburn and his co-workers have been theoretically studied using DFT in this work. On the basis of the calculations, we find that the intermolecular diamination reaction mechanism involves the dissociation of ligand, which gives active catalyst, followed by two C—N bond formation between the carbon atom of diene and nitrogen atom of urea.

In the step of C—N bond formation, each carbon atom of isoprene can react with the nitrogen atom of Pd[η^2-$(NEt)_2$CO](NCMe) or Pd[η^2-$(NEt)_2$CO]. The coupling of the terminal carbon atoms with nitrogen atom are found to be kinetically favored than the coupling between β-C atoms and nitrogen atom. The transition states, which form the first C—N bond, are the rate-determining steps in the reaction. To understand the infection of ligand number in catalyzed cycle, molecular orbital and NBO analyses are performed. The lower orbital energy difference between the fragment orbitals and the weaker coordination of Pd—N in the channels catalyzed by Pd[η^2-$(NEt)_2$CO](NCMe) makes the formation of C—N bond easier. The energy barriers of rate-determining in the channels are decreased. The reaction catalyzed by Pd[η^2-$(NEt)_2$CO](NCMe) yielding dominant product is favorable, and it is in agreement with experiments.

SUPPORTING INFORMATION

This paper contains supporting information.

Acknowledgements

This work was supported by the Key Project of Science and Technology of the Ministry of Education, P.R. China (grant No.104263).

REFERENCES

[1] D. Lucet, T. Gall, C Mioskowski,, *Angew. Chem. Int. Ed.* **1998**, *37*, 2580–2627.
[2] M. S. Mortensen, G. A. O'Doherty, *Chemtracts: Org. Chem.* **2005**, *18*, 555–561.
[3] S. R. S. S. Kotti, C. Timmons, G. Li, *Chem. Biol. Drug Des.* **2006**, *67*, 101–114.
[4] D. Lucet, T. L. Gall, C. Mioskowski, *Angew. Chem. Int. Ed.* **1998**, *37*, 2580–2672.
[5] G. Li, S. H. Kim, H. X. Wei, *Tetrahedron Lett.* **2000**, *41*, 8699–8703.
[6] P. N. Becker, M. A. White, R. G. Bergman, *J. Am. Chem. Soc.* **1980**, *102*, 5676–5677.
[7] T. P. Zabawa, D. Kasi, S. R. Chemler, *J. Am. Chem. Soc.* **2005**, *127*, 11250–11251.
[8] G. Li, H. X. Wei, S. H. Kim, M. D. Carducci, *Angew. Chem. Int. Ed.* **2001**, *40*, 4277–4280.
[9] S. Hong, T. Marks, *J. Acc. Chem. Res.* **2004**, *37*, 673–686.
[10] M. Utsunomiya, J. F. Hartwing, *J. Am. Chem. Soc.* **2004**, *126*, 2702–2703.
[11] V. I. Timokhin, N. R. Anastasi, S. S. Stahl, *J. Am. Chem. Soc.* **2003**, *125*, 12996–12997.
[12] L. S. Hegedus, *Tetrahedron* **1984**, *40*, 2415–2434.
[13] The stoichiometric Pd-mediated 1,2-diamination of alkenes was first reported in 1978: Backvall JE (1978) Tetrahedron Lett. 163.
[14] L. J. B. Gregory, G. C. Lloyd-Jones, K. I. Booker-Milburm, *J. Am. Chem. Soc.* **2005**, *127*, 7308–7309.
[15] Du. Haifeng, Zhao. Baoguo, Shi. Yian, *J. Am. Chem. Soc.* **2007**, *129*, 762–763.
[16] J. Streuff, C. H. Hovelmann, M. Nieger, K. Muniz, *J. Am. Chem. Soc.* **2005**, *127*, 14586–14587.
[17] M. J. Lee, D. S. Ahn, D. Y. Jung, J. Lee, Y. Do, Sk. Kim, S. Chang, *J. Am. Chem. Soc.* **2006**, *128*, 12954–12962.
[18] C. Lee, W. Yang, R. G. Parr, *Phys. Rev. B* **1988**, *37*, 785–789.
[19] A. D. Becke, *J. Chem. Phys.* **1993**, *98*, 5648–5652.
[20] C. Gonzalez, H. B. Schlegel, *J. Chem. Phys.* **1989**, *90*, 2154–2159.
[21] P. J. Hay, W. R. Wadt, *J. Chem. Phys.* **1985**, *82*, 270–283.
[22] W. R. Wadt, P. J. Hay, *J. Chem. Phys.* **1985**, *82*, 284–298.
[23] P. J. Hay, W. R. Wadt, *J. Chem. Phys.* **1985**, *82*, 299–310.
[24] P. J. Hariharan, J. A. Pople, *Theor. Chim. Acta* **1973**, *28*, 213–222.
[25] M. J. Frisch, G. W. Trucks, H. B. Schlegel, G. E. Scuseria, M. A. Robb, J. R. Cheeseman, J. A. Montgomery, T. Vreven, Jr K. N. Kudin, J. C. Burant, J. M. Millam, S. S. Iyengar, J. Tomasi, V. Barone, B. Mennucci, M. Cossi, G. Scalmani, N. Rega, G. A. Petersson, H. Nakatsuji, M. Hada, M. Ehara, K. Toyota, R. Fukuda, J. Hasegawa, M. Ishida, T. Nakajima, Y. Honda, O. Kitao, H. Nakai, M. Klene, X. Li, J. E. Knox, H. P. Hratchian, J. B. Cross, C. Adamo, J. Jaramillo, R. Gomperts, R. E. Stratmann, O. Yazyev, A. J. Austin, R. Cammi, C. Pomelli, J. W. Ochterski, P. Y. Ayala, K. Morokuma, G. A. Voth, P. Salvador, J. J. Dannenberg, V. G. Zakrzewski, S. Dapprich, A. D. Daniels, M. C. Strain, O. Farkas, D. K. Malick, A. D. Rabuck, K. Raghavachari, J. B. Foresman, J. V. Ortiz, Q. Cui, A. G. Baboul, S. Clifford, J. Cioslowski, B. B. Stefanov, G. Liu, A. Liashenko, P. Piskorz, I. Komaromi, R. L. Martin, D. J. Fox, T. Keith, M. A. Al-Laham, C. Y. Peng, A. Nanayakkara, M. Challacombe, P. M. W. Gill, B. Johnson, W. Chen, M. W. Wong, C. Gonzalez, J. A. Pople, **2003**, *Gaussian 03, Revision B.03*. Gaussian Inc, Pittsburgh PA.
[26] E. D. Glendening, A. E. Reed, J. E. Carpenter, F. Weinhold, NBO version 3.1.
[27] J. E. Carpenter, F. Weinhold, *J. Mol. Struct. (Theochem)* **1988**, *169*, 41–62.

[28] J. E. Charpenter, **1987**, PhD Thesis, University of Wisconsin, Madison, WI.
[29] J. P. Foster, F. Weinhold, *J. Am. Chem. Soc.* **1980**, *102*, 7211–7218.
[30] A. E. Reed, F. Weinhold, *J. Chem. Phys.* **1983**, *78*, 4066–4073.
[31] A. E. Reed, F. Weinhold, *J. Chem. Phys.* **1985**, *83*, 1736–1740.
[32] A. E. Reed, R. B. Weinstock, F. Weinhold, *J. Chem. Phys.* **1985**, *83*, 735–746.
[33] A. E. Reed, L. A. Curtiss, F. Weinhold, *Chem. Rev.* **1988**, *88*, 899–926.
[34] F. Weinhold, J. E. Carpenter, *The Structure of small molecules and ions, Plenum*: New York, **1988**, 227–236.
[35] F. Biegler-König, J. Schönbohm, R. Derdau, D. Bayles, R. F. W. Bader, *AIM 2000*, Version 1 (**2000**).
[36] S. I. Gorelsky, A. B. P. Lever, *J. Organomet. Chem.* **2001**, *635*, 187–196.
[37] S. I. Gorelsky, *AOMix: Program for Molecular Orbital Analysis*, York University, Toronto, Canada, **1997**. http://www.sf-chem.net/
[38] S. I. Gorelsky, S. Ghosh, E. I. Solomon, *J. Am. Chem. Soc.* **2006**, *128*, 278–290.